Published in "Langmuir 23(7): 3570 -3580, 2007"
which should be cited to refer to this work.

# Cluster, Glass, and Gel Formation and Viscoelastic Phase Separation in Aqueous Clay Suspensions

Andrey Shalkevich, Anna Stradner, Suresh Kumar Bhat,† François Muller,‡ and Peter Schurtenberger*

*Department of Physics and Fribourg Center for Nanomaterials, University of Fribourg, Chemin du Musée 3, CH-1700 Fribourg, Switzerland*

We have systematically investigated the phase diagram of clay particles in water to understand the relation between the local and macroscopic properties and the structures of clay suspensions. We focused, in particular, on sodium Cloisite (CNa) particles at concentrations typically used in nanocomposites (concentrations from 1 to 4 wt %) and at an extended range of ionic strengths ($10^{-5}$ to $10^{-2}$ M NaCl). The suspensions have been characterized using rheology and a combination of scattering techniques (neutrons, X-rays, and light). We demonstrate the existence of a liquid cluster phase at low clay and intermediate salt concentrations and provide new insight into the nature of the solidlike dispersions at low and high ionic strengths.



## Introduction

Recent advances in the description and understanding of aggregation, gelation, and glass formation have led to a wealth of new information in the general area of dynamical arrest and viscoelastic phase separation.[1−4] Phase transitions involving, for example, purely repulsive or strongly attractive interactions are now well established for charged spherical particles (silica, latex).[5,6] Moreover, new equilibrium cluster phases have been discovered for colloidal suspensions and protein solutions, where the particles interact via a combination of short-range attractive and long-range repulsive forces.[7] This is not the case for charged anisotropic colloids, for example, disclike clay particles, where the status of the state diagram is still under considerable debate in the literature.[8−20]

The gelation of dispersions of clay particles is both industrially important and of theoretical interest. Clay gels have applications in drilling fluids, paints, ceramic additives, and in cosmetic and pharmaceutical formulations. Over more than 50 years, various gelation mechanisms and suspension structures have been proposed for clays. Van Olphen proposed that clay dispersions may form three-dimensional, aggregated structures, a so-called "house of cards".[21,22] This structure was believed to come from electrostatic attraction between oppositely charged double layers at the edges and faces of the particles as a result of the different chemical composition of the face and edge surfaces. The face has a constant negative charge due to substitution within the clay lattice. The edges are like oxide surfaces; therefore, they may be positively or negatively charged depending on the pH of the dispersion.

Most recent studies of clay gel structures have been carried out using commercially available synthetic samples of Laponite, which consists of disclike particles with a thickness of 1 nm and an average diameter of ∼30 nm. Laponite is a three-layer clay composed of a central octahedrally coordinated magnesium−oxygen−hydroxide sheet sandwiched between two tetrahedrally coordinated silica−oxygen sheets. Isomorphic substitutions of

* To whom correspondence should be addressed. Fax: (+41)263009747. E-mail: Peter.Schurtenberger@unifr.ch.

† Present address: Polymer Science and Engineering Division, National Chemical Laboratory, Pune−411008, India.

‡ Present address: Institute of Chemistry, Heinrichstr. 28, University of Graz, AT-8010 Graz, Austria.

(1) Tanaka, H. Viscoelastic phase separation. *J. Phys.: Condens. Matter.* **2000**, *12* (15), R207.

(2) Trappe, V.; Sandkühler, P. Colloidal gels−low-density disordered solid-like states. *Curr. Opin. Colloid Interface Sci.* **2004**, *8*, 494−500.

(3) Bergenholtz, J.; Fuchs, M.; Voigtmann, T. Colloidal gelation and non-ergodicity transitions. *J. Phys.: Condens. Matter* **2000**, *12* (29), 6575.

(4) Segrè, P. N.; Prasad, V.; Schofield, A. B.; Weitz, D. A. Glasslike Kinetic Arrest at the Colloidal-Gelation Transition. *Phys. Rev. Lett.* **2001**, *86*, 6042−6045.

(5) Dietler, G.; Aubert, C.; Cannell, D. S. Gelation of Colloidal Silica. *Phys. Rev. Lett.* **1986**, *57*, 3117.

(6) Beck, C.; Hartl, W.; Hempelmann, R. The glass transition of charged and hard sphere silica colloids. *J. Chem. Phys.* **1999**, *111* (17), 8209.

(7) Stradner, A.; Sedgwick, H.; Cardinaux, F.; Poon, W. C. K.; Egelhaaf, S. U.; Schurtenberger, P. Equilibrium cluster formation in concentrated protein solutions and colloids. *Nature* **2004**, *432* (7016), 492.

(8) Knaebel, A.; Bellour, M.; Munch, J.-P.; Viasnoff, V.; Lequeux, F.; Harden, J. L. Aging behavior of Laponite clay particle suspensions. *Europhys. Lett.* **2000**, *52* (1), 73.

(9) Tombácz, E.; Szekeres, M. Colloidal behavior of aqueous montmorillonite suspensions: the specific role of pH in the presence of indifferent electrolytes. *Appl. Clay Sci.* **2004**, *27* (1−2), 75.

(10) Bonn, D.; Tanaka, H.; Wegdam, G.; Kellay, H. J. M. Aging of a colloidal "Wigner" glass. *Europhys. Lett.* **1998**, *45* (1), 52.

(11) Kroon, M.; Wegdam, G. H.; Sprik, R. Dynamic light scattering studies on the sol-gel transition of a suspension of anisotropic colloidal particles. *Phys. Rev. E* **1996**, *54*, 6541.

(12) Trizac, E.; Bocquet, L.; Agra, R.; Weis, J. J.; Aubouy, M. Effective interactions and phase behaviour for a model clay suspension in an electrolyte. *J. Phys.: Condens. Matter* **2002**, *14* (40), 9339.

(13) Ruzicka, B.; Zulian, L.; Ruocco, G. Ergodic to non-ergodic transition in low concentration Laponite. *J. Phys.: Condens. Matter* **2004**, *16* (42), S4993.

(14) Dijkstra, M.; Hansen, J. P.; Madden, P. A. Gelation of a Clay Colloid Suspension. *Phys. Rev. Lett.* **1995**, *75* (11), 2236.

(15) Tanaka, H.; Jabbari-Farouji, S.; Meunier, J.; Bonn, D. Kinetics of ergodic-to-nonergodic transitions in charged colloidal suspensions: Aging and gelation. *Phys. Rev. E* **2005**, *71* (2), 021402.

(16) Bonn, D.; Kellay, H.; Tanaka, H.; Wegdam, G.; Meunier, J. Laponite: What Is the Difference between a Gel and a Glass? *Langmuir* **1999**, *15* (22), 7534.

(17) Tanaka, H.; Meunier, J.; Bonn, D. Nonergodic states of charged colloidal suspensions: Repulsive and attractive glasses and gels. *Phys. Rev. E* **2004**, *69* (3), 031404.

(18) Mourchid, A.; Delville, A.; Lambard, J.; LeColier, E.; Levitz, P. Phase Diagram of Colloidal Dispersions of Anisotropic Charged Particles: Equilibrium Properties, Structure, and Rheology of Laponite Suspensions. *Langmuir* **1995**, *11* (6), 1942.

(19) Michot, L. J.; Bihannic, I.; Porsch, K.; Maddi, S.; Baravian, C.; Mougel, J.; Pierre, L. Phase Diagrams of Wyoming Na-Montmorillonite Clay. Influence of Particle Anisotropy. *Langmuir* **2004**, *20* (25), 10829.

(20) Ruzicka, B.; Zulian, L.; Ruocco, G. More on the Phase Diagram of Laponite. *Langmuir* **2006**, *22* (3), 1106−1111.

(21) Van Olphen, H. *An Introduction to Clay Colloid Chemistry*; Wiley and Sons: New York, 1997.

(22) Van Olphen, H. Rheological phenomena of clay sols in connection with the charge distribution on the micelles. *Discuss. Faraday Soc.* **1951**, *11*, 82−84.

the divalent magnesium atoms by monovalent lithium lead to the formation of negative charges within the lattice, which is balanced by the sodium ions located at the surface.

Small-angle X-ray scattering (SAXS),[23−26] small-angle neutron scattering (SANS),[27−30] static and dynamic light scattering (SLS and DLS),[8,11,31−38] rheology,[18,30,32,39,40] scanning and transmission electron microscopy (SEM and TEM),[41] and nuclear magnetic resonance (NMR)[42] have been applied to clay suspensions to investigate Van Olphen's house-of-cards structure in Laponite dispersions.

An alternative structure to the house-of-cards structure discussed above has been proposed to account for gelation in clay dispersions at low ionic strengths. Norrish found evidence for regular spacing between clay particles in concentrated dispersions.[43] The distance between the particles, determined by X-ray diffraction, increased with decreasing electrolyte concentration. Norrish proposed that solidification could result from electrical double-layer repulsion between clay particles, leading to the formation of a Wigner glass. Further evidence for such a Wigner glass at low electrolyte concentrations came from the rheological measurements of Rand et al.[44] and from many other experiments.[10,13,25,45]

By contrast, it has recently been hypothesized that Laponite suspensions could behave like an attractive glass.[17] A comprehensive discussion of different possible glassy states in Laponite suspensions, including comparison with experimental data, was recently given by Mongondry et al.[46] and Tanaka et al.[15,17]

The majority of clay gelation studies have been done with Laponite suspensions due to their relatively high longitudinal monodispersity in comparison with natural clays. However, direct observation of Laponite with atomic force microscopy (AFM) or electron microscopy (EM) shows that Laponite exhibits a considerable polydispersity.[47−49] At the same time, Laponite is chemically unstable at pH <10. Contrary to Laponite, the commercially available natural clay montmorillonite is stable even at very low pH, which allows one to study montmorillonite in a wide range of pHs and ionic strengths. Montmorillonite particles have aspect ratios of the order 100:1, which is much higher than those for Laponite, and therefore the edge area for montmorillonite is typically a very small proportion (<1%) of the total surface area of the particles. The edge surface area is thus expected to be less important in determining the particle interactions in montmorillonite dispersions.

The present work investigates the effects of ionic strength on the structural and dynamic properties of different phases found in montmorillonite dispersions. By this means, we sought to establish whether there are one or more types of internal particle organization in montmorillonite dispersions and, in particular, to critically examine the different structures and mechanisms, such as the house-of-cards structure or Wigner or attractive glasses, proposed for the formation of solids as a function of the ionic strength. As this requires access to a very large range of length and time scales, we combined different scattering techniques and rheological measurements.

## Experimental Methods

**A. Materials.** We used the sodium montmorillonite clay Cloisite CNa (Southern Clay Products, Inc., Gonzales, TX). The cation exchange capacity is 0.98 mequiv/g, which yields a charge density of 0.01 e/Å$^2$ (i.e., $\sim 3 \times 10^4$ charges per face). Cloisite CNa particles were reported to be discrete platelike crystals with a diameter of a few hundred nanometers and a thickness of 1 nm.[50]

The suspensions were prepared as follows. The clay powder was slowly mixed in Milli-Q water or $D_2O$ at a certain mass fraction (2 and 4 wt %) and then stirred for 1 h with a magnetic stirrer. After that, mixed-bed ion exchange resin was added for 1 week to remove the excess ions. Once the resins were mixed with the suspensions, we periodically agitated the sample tube. Afterward, the dispersions were filtered through 5 $\mu$m pore size Millipore filters, which removed all the ion exchanger beads. Removing the excess salt by means of an ion exchanger leads to a decrease in the pH of the clay suspension


(23) Saunders, J. M.; Goodwin, J. W.; Richardson, R. M.; Vincent, B. A. Small-Angle X-ray Scattering Study of the Structure of Aqueous Laponite Dispersions. *J. Phys. Chem. B* **1999**, *103* (43), 9211.

(24) Lemaire, B. J.; Panine, P.; Gabriel, J. C. P.; Davidson, P. The measurement by SAXS of the nematic order parameter of laponite gels. *Europhys. Lett.* **2002**, *59* (1), 55.

(25) Levitz, P.; Lecolier, E.; Mourchid, A.; Delville, A.; Lyonnard, S. Liquid-solid transition of Laponite suspensions at very low ionic strength: Long-range electrostatic stabilisation of anisotropic colloids. *Europhys. Lett.* **2000**, *49* (5), 672.

(26) Michot, L. J.; Bihannic, I.; Maddi, S.; Funari, S. S.; Baravian, C.; Levitz, P.; Davidson, P. Liquid-crystalline aqueous clay suspensions. *Proc. Natl. Acad. Sci. U.S.A.* **2006**, *103* (44), 16101−16104.

(27) Avery, R. G.; Ramsay, J. D. F. Colloidal properties of synthetic hectorite clay dispersions II. Light and small angle neutron scattering *J. Colloid Interface Sci.* **1986**, *109* (2), 448.

(28) Martin, C.; Pignon, F.; Piau, J.-M.; Magnin, A.; Lindner, P.; Cabane, B. Dissociation of thixotropic clay gels. *Phys. Rev. E* **2002**, *66* (2), 021401.

(29) Pignon, F.; Magnin, A.; Piau, J.-M.; Cabane, B.; Lindner, P.; Diat, O. Yield stress thixotropic clay suspension: Investigations of structure by light, neutron, and x-ray scattering. *Phys. Rev. E* **1997**, *56*, 3281.

(30) Pignon, F.; Magnin, A.; Piau, J.-M. Thixotropic behavior of clay dispersions: Combinations of scattering and rheometric techniques. *J. Rheol.* **1998**, *42* (6), 1349.

(31) Abou, B.; Bonn, D.; Meunier, J. Aging dynamics in a colloidal glass. *Phys. Rev. E* **2001**, *64*, 021510.

(32) Pignon, F.; Magnin, A.; Piau, J.-M. Butterfly Light Scattering Pattern and Rheology of a Sheared Thixotropic Clay Gel. *Phys. Rev. Lett.* **1997**, *79* (23), 4689.

(33) Ruzicka, B.; Zulian, L.; Ruocco, G. Routes to Gelation in a Clay Suspension. *Phys. Rev. Lett.* **2004**, *93* (25), 258301.

(34) Pignon, F.; Piau, J.-M.; Magnin, A. Structure and Pertinent Length Scale of a Discotic Clay Gel. *Phys. Rev. Lett.* **1996**, *76* (25), 4857.

(35) Kroon, M.; Vos, W. L.; Wegdam, G. H. Structure and formation of a gel of colloidal disks. *Phys. Rev. E* **1998**, *57*, 1962.

(36) Nicolai, T.; Cocard, S. Dynamic Light-Scattering Study of Aggregating and Gelling Colloidal Disks. *J. Colloid Interface Sci.* **2001**, *244* (1), 51.

(37) Rostaa, L.; von Gunten, H. R. Light scattering characterization of laporite sols. *J. Colloid Interface Sci.* **1990**, *134* (2), 397.

(38) Wu, H.; Xie, J.; Lattuada, M.; Morbidelli, M. Scattering Structure Factor of Colloidal Gels Characterized by Static Light Scattering, Small-Angle Light Scattering, and Small-Angle Neutron Scattering Measurements. *Langmuir* **2005**, *21* (8), 3291.

(39) Axford, S. D. T.; Herrington, T. M. Determination of aggregate structures by combined light-scattering and rheological studies. *J. Chem. Soc., Faraday Trans.* **1994**, *90* (14), 2085.

(40) Pignon, F.; Magnin, A.; Piau, J.-M. Thixotropic colloidal suspensions and flow curves with minimum: Identification of flow regimes and rheometric consequences. *J. Rheol.* **1996**, *40* (4), 573.

(41) Bihannic, I.; Michot, L. J.; Lartiges, B. S.; Vantelon, D.; Labille, J.; Thomas, F.; Susini, J.; Salomé, M.; Fayard, B. First Direct Visualization of Oriented Mesostructures in Clay Gels by Synchrotron-Based X-ray Fluorescence Microscopy. *Langmuir* **2001**, *17* (14), 4144−4147.

(42) Levitz, P. E.; Korb, J.-P. Probing glass transition of clay colloids by NMR relaxometry: Interplay between fluid Brownian dynamics and particle jamming. *Europhys. Lett.* **2005**, *70* (5), 684−689.

(43) Norrish, K. The swelling of montmorillonite. *Discuss. Faraday Soc.* **1954**, *18*, 120−134.

(44) Rand, B.; Peken, E.; Goodwin, J. W.; Smith, R. W. Investigation into the existence of edge−face coagulated structures in Na-montmorillonite suspensions. *J. Chem. Soc., Faraday Trans. 1* **1980**, *76*, 225−235.

(45) Mourchid, A.; Levitz, P. Long-term gelation of laponite aqueous dispersions. *Phys. Rev. E* **1998**, *57*, R4887.

(46) Mongondry, P.; Tassin, J. F.; Nicolai, T. Revised state diagram of Laponite dispersions. *J. Colloid Interface Sci.* **2005**, *283* (2), 397−405.

(47) Balnois, E.; Durand-Vidal, S.; Levitz, P. Probing the Morphology of Laponite Clay Colloids by Atomic Force Microscopy. *Langmuir* **2003**, *19* (17), 6633−6637.

(48) Leach, E. S. H.; Hopkinson, A.; Franklin, K.; van Duijneveldt, J. S. Nonaqueous Suspensions of Laponite and Montmorillonite. *Langmuir* **2005**, *21* (9), 3821−3830.

(49) Negrete, H. N.; Letoffe, J. M.; Putaux, J. L.; David, L.; Bourgeat-Lami, E. Aqueous Dispersions of Silane-Functionalized Laponite Clay Platelets. A First Step toward the Elaboration of Water-Based Polymer/Clay Nanocomposites. *Langmuir* **2004**, *20* (5), 1564−1571.

(50) Physical Properties Bulletin from Southern Clay Products, Inc., Gonzales, TX.

from an initial value of pH 11 for fresh 2 wt % to a value of ∼4 in the final suspension. In the case of a 4 wt % suspension, the drift of the pH is even larger: it drifts from 12 down to 3.7. In contrast to natural suspensions, where the pH is very sensitive to salt concentration and clay content, under acidic conditions, the pH and therefore the surface charge of montmorillonite suspensions are independent of the salt and clay concentrations in the entire experimentally accessible range. Another advantage of acidic conditions is a high aggregation stability for most of the studied suspensions (except for the phase-separated samples): Cloisite samples stay for more than 1 year without any sedimentation, while the natural suspensions of Cloisite were flocculated after a maximum of a few months independently of salt and clay content.

The final dispersions were prepared by diluting the stock suspensions. For suspensions with a low concentration, we used a stock of 2 wt %, whereas for samples with a montmorillonite content above 2 wt %, a stock concentration of 4 wt % was used. A NaCl solution was then added to obtain the required salt content. The salt concentration after the ion exchange process was estimated to be as small as $10^{-5}$ M, and the salt content indicated in the text takes into account added salt only. Finally, shortly before filling the cell, the suspensions were ultrasonicated for a few minutes at 50% amplitude with a Branson sonifier 250, while the vial was cooled in an ice bath to prevent overheating during sonication. The aging of the samples was then examined as a function of time, where the end of sonication was taken as $t = 0$.

**B. Methods.** The phase diagram was determined by a combination of visual observations and rheological measurements. Initially, some of the samples exhibited a slow variation of the viscosity with time. Therefore, all dispersions were kept under the same conditions for 3 months before they were experimentally investigated. This time delay was chosen based on small-angle light scattering data which show no evolution in time after 2 months.

The rheological behavior of clay dispersions was studied with a MCR 300 rheometer (Paar Physica) in a temperature-controlled narrow-gap Mooney−Ewart geometry. Measurements of the storage ($G'$) and loss ($G''$) moduli were performed in an angular frequency range of $10^{-1} < \omega < 10^{2}$ rad/s. All tests were done at 25 °C.

The small-angle neutron scattering experiments were carried out using the SANS I instrument at the Paul Scherrer Institute (PSI) in Villigen, Switzerland. Samples were inserted into circular quartz cells from Helma with a path length of 2 mm, and a thermostated sample holder was used. The combination of different wavelengths (0.8 and 1.267 nm), sample-to-detector distances (4.5−20 m), and collimation lengths (4.5−18 m) resulted in a $q$-range of 0.007−1.5 $nm^{-1}$. The raw data were corrected for background from the solvent, sample cell, and electronic noise by conventional procedures.[51] Furthermore, the two-dimensional isotropic scattering spectra were azimuthally averaged, converted to absolute scale, and corrected for detector efficiency by dividing with the incoherent scattering spectra of a water standard.[52]

Small-angle light scattering (SALS) experiments were carried out using a home-built instrument similar to one described in detail elsewhere.[53] A linearly polarized He−Ne laser (Melles Griot) of 2 mW output power operating at a wavelength of 632.8 nm was used as the light source. The beam was expanded to a diameter of 9 mm using a beam expander to match the speckle size and the pixel size of the CCD camera. The collimated beam was directed onto the sample contained in a rectangular cuvette (Hellma) with a path length of 1−2 mm. The transmitted light as well as the scattered light was collected by a Fourier lens of 100 mm focal length in whose focal plane a beam stop of 1 mm diameter was placed to block the transmitted beam. A second lens collected the scattered light around the beam stop and imaged it onto the detector with a unit magnification. With this scheme, each CCD pixel corresponds to a different scattering vector $q$ and scattering vectors of the same magnitude are mapped to the pixels lying on a circle centered about the optic axis. The CCD detector used is a 10-bit digital camera (Pulnix TM1300) with a 1360 × 1034 pixel sensor, with each pixel being 6.7 × 6.7 $\mu m^2$. The maximum speed of the camera is 12 frames/s. The digitized images were acquired using a frame grabber (Matrox Meteor II/Digital) and processed using a PC. The angular range accessible with this instrument is between 0.09° and 5°, which corresponds to a scattering vector range of $2 \times 10^{-5} < q < 1.2 \times 10^{-3}$ $nm^{-1}$. To obtain the scattered intensity $I(q)$, the CCD output was averaged over rings of pixels centered about the optical axis and the measurements were corrected for the contribution from the CCD dark noise and the stray light.

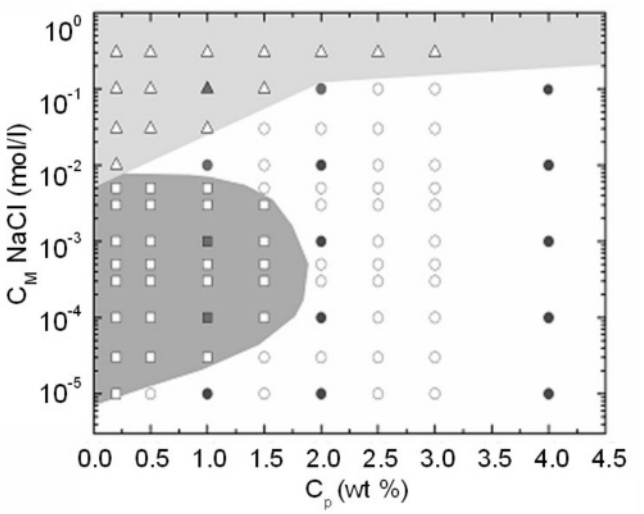


**Figure 1.** Macroscopic state diagram of aqueous clay suspensions. Solid phases are indicated by circles, liquid phases by squares, and phase-separated systems by triangles. Filled symbols indicate detailed investigations using SANS (see text for details).

Environmental scanning electron microscopy (ESEM), providing a controlled humidity sample environment by means of a specially designed cooling stage, was performed on a Phillips XL30 FEG instrument operating in ESEM mode. A brief overview of the applications of ESEM to colloids can be found in ref 54. The moisture content of the clay dispersion was adjusted to a desired humidity by a built-in cooling stage in the ESEM chamber. All images were obtained at 4 °C, and the pressure was altered to 3 Torr to maintain humidities around 80%.

## Results

**A. State Diagram Based on Visual Observation and Viscoelastic Properties.** The phase behavior of colloidal clay particles suspended in water has attracted considerable attention in the past, and a number of different states, such as gels, glasses, viscous fluids, or phase-separated flocks, have been reported in the literature.[17,55,56] Here, we present results from a systematic investigation of the structural and dynamic properties of aqueous dispersions of montmorillonite particles, where the concentration of clay and added salt has been varied. The results are summarized in Figure 1, where we show the state diagram based on visual inspection and rheological measurements. Figure 1 describes the

(51) Cotton, J. P. Introduction to an Investigative Tool For Colloidal and Polymeric Systems. In *Neutrons, X-Ray and Light Scattering*; Lindner, P., Zemb, T., Eds.; North-Holland: Amsterdam, 1991.

(52) Wignall, G. D.; Bates, F. S. Absolute calibration of small-angle neutron scattering data. *J. Appl. Crystallogr.* **1987**, *20* (1), 28−40.

(53) Luca, C.; Weitz, D. A. Ultralow-angle dynamic light scattering with a charge coupled device camera based multispeckle, multitau correlator. *Rev. Sci. Instrum.* **1999**, *70* (8), 3214−3221.

(54) Donald, A. M. Environmental scanning electron microscopy for the study of "wet" systems. *Curr. Opin. Colloid Interface Sci.* **1998**, *3* (2), 143−147.

(55) Fossum, J. O. Physical phenomena in clays. *Physica A* **1999**, *270* (1−2), 270.

(56) Mourchid, A.; Lécolier, E.; Van Damme, H.; Levitz, P. On Viscoelastic, Birefringent, and Swelling Properties of Laponite Clay Suspensions: Revisited Phase Diagram. *Langmuir* **1998**, *14* (17), 4718.

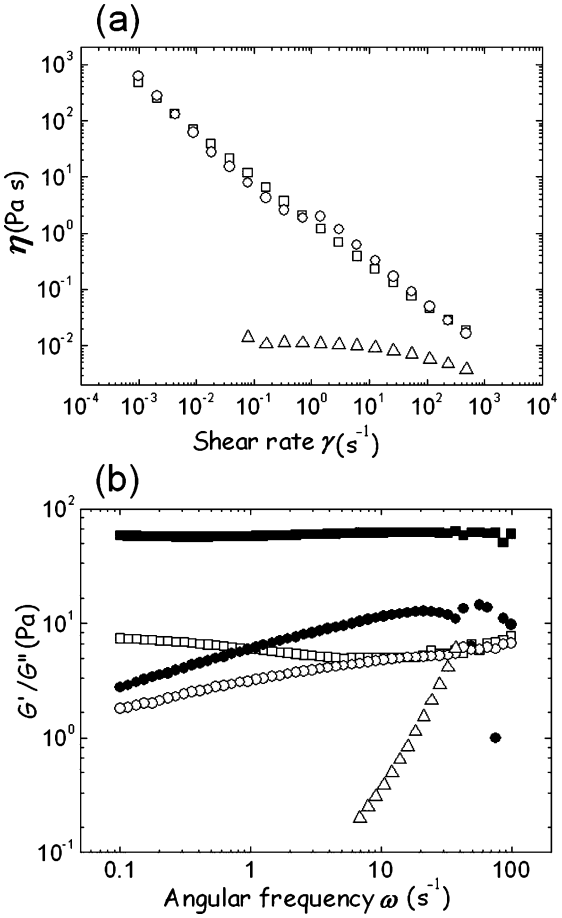


**Figure 2.** (a) Viscosity as a function of shear rate for Cloisite CNa suspensions of $c = 1$ wt % and $10^{-5}$ M NaCl (circles), $10^{-4}$ M NaCl (triangles), or $10^{-2}$ M NaCl (squares). (b) Frequency response of the storage ($G'$, filled symbols) and loss ($G''$, open symbols) moduli for a Cloisite CNa suspension of $c = 1$ wt % and $10^{-5}$ M NaCl (circles), $10^{-4}$ M NaCl (triangles), or $10^{-2}$ M NaCl (squares).

appearance of liquid- and solidlike states as a function of ionic strength and clay concentration. It is important to point out that the data shown in Figure 1 represent a "state" diagram with regions that do not correspond to equilibrium but rather to nonequilibrium solid states such as glasses and/or gels.

Three distinct regions are observed: (1) The majority of samples investigated exhibit solidlike properties (circles); that is, these samples possess measurable bulk elasticity. (2) At intermediate salt and low particle concentrations, we observe typical liquidlike behavior (squares), with a viscosity comparable to that of pure water. (3) At high salt and low and intermediate particle concentrations (triangles), we finally observe flocculation and macroscopic phase separation. The distinction between liquid- and solidlike behavior is, in general, easily made for most of the samples investigated. However, at low clay concentrations, neither simple visual inspection nor dynamic light scattering (DLS) is able to provide any evidence for the dynamical arrest transition indicated in Figure 1. All samples investigated in this region of the state diagram appear to be completely ergodic on the length and time scales accessible in DLS. It is only from rheological measurements that we are able to draw the part of the solid−liquid state (or glass) boundary found at salt concentrations between $10^{-5}$ and $10^{-4}$ M NaCl and at clay concentrations below 2 wt %. This is illustrated in Figure 2, where we plot some examples of the shear rate dependence of the viscosity and the frequency-dependent loss and storage moduli obtained for $c =$ 1 wt % and increasing salt concentration. All rheological results are fully reproducible.

This figure clearly demonstrates the existence of a re-entrant solid formation or dynamical arrest as a function of increasing salt concentration for a clay concentration of 1 wt %. At an intermediate ionic strength of $10^{-4}$ M NaCl, we find that the flow curve exhibits a plateau viscosity at low shear rates, before shear thinning can be observed at higher shear rates as shown in Figure 2a. Owing to the small particle size, Brownian motion is very effective in keeping the system close to equilibrium, and we have to apply rather large shear rates before shear thinning sets in. At low ionic strength, that is, in the completely deionized state, the situation completely changes. No Newtonian plateau can be found in the experimentally accessible range of shear values, and the sample exhibits the shear-thinning behavior shown in Figure 2a with $\eta \propto \gamma^{-1}$ over more than five decades in $\gamma$, similar to what has been observed previously in colloidal suspensions exhibiting solidlike behavior.[57] Applying a steady shear to these solidlike samples causes the configuration of the platelets to yield; this yielding results in the shear-thinning behavior shown in Figure 2a. A similar behavior is again found at higher salt concentrations, where, once again, a solidlike state with a finite dynamical yield stress value and shear thinning with $\eta \propto \gamma^{-1}$ over more than five decades in $\gamma$ can be observed. These findings are supported by frequency-dependent oscillatory measurements as shown in Figure 2b. For the dynamically arrested samples at low and high ionic strengths, the small-amplitude dynamic response (Figure 2b) exhibits solidlike behavior with a storage modulus $G'(\omega)$ that exceeds the loss modulus $G''(\omega)$ over the measured range of angular frequency ($\omega$). For the liquid state at $10^{-4}$ M NaCl, we observe typical liquidlike behavior, where $G''(\omega)$ increases linearly with $\omega$ and $G'(\omega)$ is too small to be measured.

It is noteworthy that the frequency-dependent response of the solidlike samples exhibits distinct differences. For the solidlike sample at high ionic strength, $G'(\omega)$ is significantly higher than that for the solidlike sample at low ionic strength. Moreover, $G'(\omega)$ remains nearly frequency-independent for the sample at $10^{-2}$ M NaCl, while we find that $G'(\omega)$ slowly decreases with decreasing $\omega$ for the sample at $10^{-5}$ M NaCl.

These findings seemingly indicate a change in the origin of the stress-bearing properties depending on whether the solid is formed at low or high ionic strength.

This first series of experiments thus indicates a state diagram of Cloisite in water that exhibits a relatively small region of liquidlike behavior at intermediate salt and low clay concentrations. The liquid region becomes narrower at higher clay concentrations and finally disappears for $c \approx 2.0$ wt %. At a high salt content above approximately 0.01−0.1 M NaCl, Cloisite appears to be unstable, and flocculation and macroscopic phase separation can be observed. The line separating the phase separation regime from the macroscopically homogeneous solidlike region appears to depend on clay concentration and moves to higher ionic strength for larger $c$-values. The state diagram shown in Figure 1 is comparable to the schematic phase diagram of Laponite published by Tanaka and collaborators,[17] where they postulated the existence of three different types of solidlike amorphous phases. They described a state diagram with a repulsive glass at low ionic strength, an attractive glass at intermediate strength, and a gel phase at high ionic strength, separated by a liquid region at a low Laponite concentration. In

(57) Zackrisson, M.; Stradner, A.; Schurtenberger, P.; Bergenholtz, J. Structure, dynamics, and rheology of concentrated dispersions of poly(ethylene glycol)-grafted colloids. *Phys. Rev. E* **2006**, *73* (1), 011408.

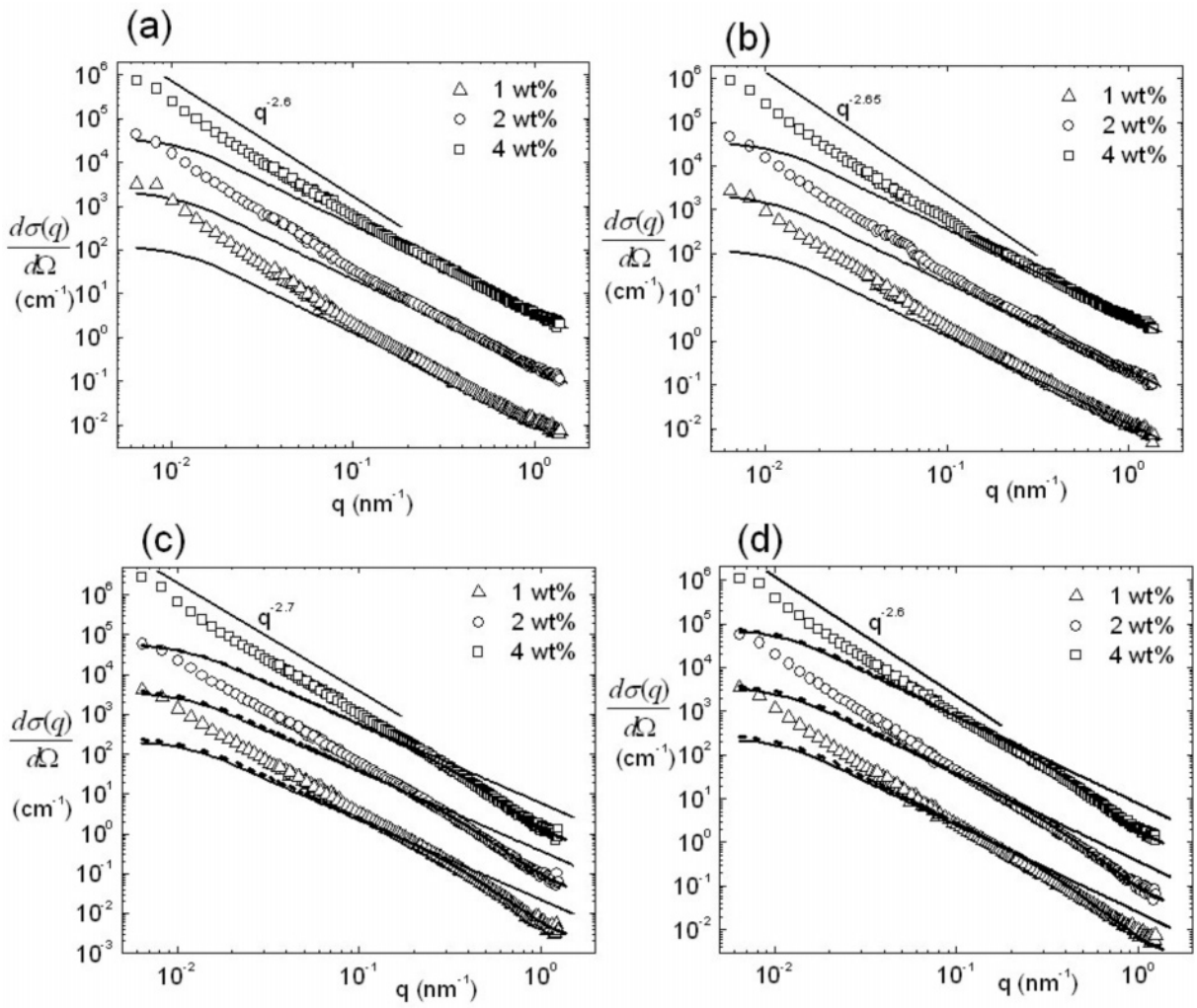


**Figure 3.** Neutron small-angle scattering data collected for Cloisite CNa suspensions at different solid concentrations and (a) $10^{-3}$ M NaCl, (b) fully deionized, (c) $10^{-2}$ M NaCl, or (d) $10^{-1}$ M NaCl. The solid lines represent the calculated form factor of polydisperse thin discs with a Gaussian polydispersity in radius of 20% with a radius of 100 nm and a thickness of 1 nm. $\rho$(CNa) = $3.82 \times 10^{10}$ cm$^{-2}$, $\rho(D_2O)$ = $6.33 \times 10^{10}$ cm$^{-2}$. The dash-dotted curves are the calculated form factor of stacked discs with 5 discs per stack.

addition, they also postulated the existence of a region of phase separation at high ionic strength. However, it is clear that our macroscopic investigations do not allow us to conclude on the natures and the underlying structures of the different states. Therefore, we also performed a series of scattering experiments where we combined small-angle light and neutron scattering to cover the required extremely large range of characteristic length scales.

**B. Small-Angle Neutron Scattering.** Suspensions of montmorillonite at different concentrations and salt content were investigated with SANS. We measured samples from all the different regions in the state diagram, indicated as solid points in Figure 1. The scattering data from these montmorillonite dispersions with different salt concentrations are shown in Figure 3. At first, all these curves look disappointingly similar, despite the fact that they were obtained with samples that exhibit very different dynamic properties. However, a closer look at the data reveals small but significant differences that can be used to help understand the underlying structures of the liquid- and solidlike dispersions. This is best illustrated with a comparison of the data to the theoretical scattering curves from isolated and fully exfoliated clay particles. These scattering curves were calculated assuming randomly oriented polydisperse discs with a mean radius of 100 nm and a thickness of 1 nm.

We first look at the data obtained with the liquidlike sample, that is, a clay suspension with 1 wt % clay particles and $10^{-3}$ M NaCl (Figure 3a). Here, we could expect good agreement between the data and the theoretical form factor for individual clay particles. At high $q$-values, the agreement is indeed quantitative, indicating that the suspension contains fully exfoliated clay particles. However, at low values of $q$, we see a clear disagreement, and the data do not exhibit the typical crossover from the $q^{-2}$ behavior for thin discs to the Guinier regime expected for particles with an average radius of 100 nm. Instead, we observe a crossover to another power law regime, where the scattering intensity is proportional to $q^{-2.6}$. This is a clear sign that the individual clay particles are not isolated but are part of much larger clusters or aggregates with at least a locally fractal structure. We are thus confronted with a situation where the individual clay particles form clusters immediately after sonication, with a relatively dense but fractal-like structure. The average size of these clusters cannot be determined with SANS, as there is no sign of a crossover to a Guinier regime in the accessible range of scattering vectors. Nevertheless, it is clear that these cluster structures are much larger than the average size of the clay discs obtained from cryo-TEM experiments on the same clay particles.[58] Moreover, additional dynamic and static light scattering experiments with much more diluted samples (*c*

$= 10^{-4}$ wt %) at the same ionic strength have also indicated the presence of large fractal clusters under these conditions (data not shown).

At higher clay concentrations, the samples with a salt concentration of $10^{-3}$ M NaCl are now in the solid region of the state diagram. This dramatic change in the dynamic properties of the samples is not reflected in the SANS data, indicating that the dynamic arrest that occurs at increasing particle concentrations is not accompanied by any dramatic variation in the local particle structure. This lack of a structural change upon the dynamic arrest transition that can be observed in these suspensions also becomes evident at the lowest ionic strength investigated (Figure 3b). All fully deionized samples investigated exhibit solidlike dynamic behavior, yet at first sight, we again observe no difference compared to the data measured in the liquid sample. In all of these samples, we find evidence for fully exfoliated clay discs that aggregate to large clusters with a rather dense fractal structure characterized by a fractal dimension of ~2.6.

However, the situation changes at a higher ionic strength, as demonstrated by the data shown in Figure 3c and d. Here, we look either at solidlike structures at all concentrations for an ionic strength of $10^{-2}$ M NaCl (Figure 3c) or at a transition from flocculation and phase separation for 1 wt % clay to dynamically arrested systems at higher clay concentrations for an ionic strength of 0.1 M NaCl (Figure 3d). At first, all the data sets look very similar again. However, a comparison with the theoretical form factor for isolated clay particles clearly indicates that we no longer have clusters of fully exfoliated discs but rather of stacks. The fractal structure is still present, as seen from the power law dependence of the scattering data at $q \leq 0.1$ nm$^{-1}$, but the building blocks are no longer single discs but rather entire stacks of discs. Fitting the SANS data using a model of stacks of discs[59] gives a small number of 5 or 6 discs per stack with a high stacking disorder, that is, a significant variation of the interlayer distances. The agreement between this model and the experimental data is also indicated in Figure 3c and d. This ability of our suspensions to form different building blocks depending on ionic strength provides additional evidence that we are indeed able to fully disperse our clay particles by sonication and that the structures subsequently formed are equilibrium by nature.

There still remains a signature in the scattering data that we have not yet discussed. As seen in Figure 3a and b, the data at low ionic strength exhibit a weak shoulder at a $q$-value of ~0.07−0.1 nm$^{-1}$. This is the result of an underlying peak in the structure factor arising from local positional correlations between the individual clay particles in the clusters. This peak becomes much more visible when calculating an effective structure factor defined as $S_{\text{eff}} = I(q)/P(q)$, where $I(q)$ is the scattered intensity and $P(q)$ is the theoretical form factor of an individual disc with a radius of 100 nm and a thickness of 1 nm. The corresponding curves are shown in Figure 4, and we observe clearly visible peaks for higher clay concentrations of 2 and 4 wt %, which are completely absent at the lowest concentrations investigated. It is interesting to note that the peak position seems to depend on the clay concentration and not on the ionic strength. The ionic strength appears to influence the peak height, that is, the degree of correlation, but not the characteristic length scale of the structural correlations. A qualitative estimate of this characteristic distance using $d \approx 2\pi/q^*$, where $q^*$ is the position of the peak in the effective structure factor, yields values of about 100 nm at $c =$ 2 wt % and 70 nm at $c = 4$ wt %. However, it is important to point out that the experimentally observed effective structure factors $S_{\text{eff}}(q)$ are the result of a convolution of the "real" structure factor $S(q)$ with the instrument resolution function; that is, $S_{\text{eff}}(q)$ is strongly smeared and we can expect the actual peaks in $S(q)$ to be much more pronounced and significantly narrower. However, due to the lack of an appropriate model for $S(q)$, we have not attempted to perform a deconvolution of $S_{\text{eff}}(q)$.

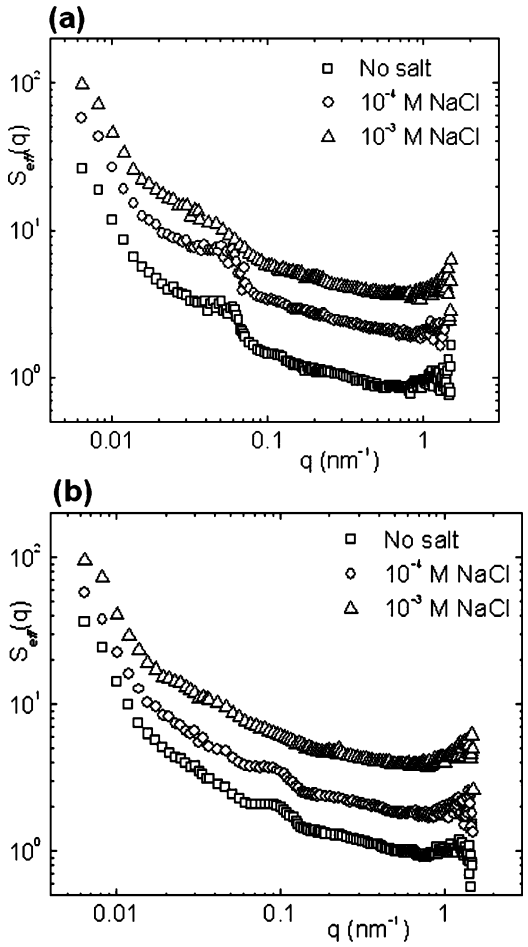


**Figure 4.** Effective structure factor $S_{\text{eff}}(q)$ of Cloisite CNa suspensions at different salt concentrations and (a) 2 wt % or (b) 4 wt % of CNa measured with neutron scattering as a function of the scattering wave vector.

Summarizing the SANS data obtained with samples from the different regions of the state diagram in Figure 1, we observe full exfoliation of the clay particles at low salt concentrations ($I_0 \leq 10^{-3}$ M only). However, these discs are not suspended as individual particles, but they form large clusters or system-spanning networks with a rather dense fractal structure described by a fractal exponent of $d_F \approx 2.6$.

These clusters then form either a solidlike or liquidlike suspension, depending upon both the clay and salt concentrations. Moreover, the individual platelets in the clusters are not arranged in a completely random fashion but exhibit structural correlations over a characteristic distance of ~70−100 nm, depending upon the clay concentration. At higher salt concentrations, the particles are no longer fully exfoliated but are present as stacks that now form the building blocks of the fractal clusters or system-spanning networks still present at all concentrations. However, from these experiments, it has also become clear that, due to the restricted accessible length scales, SANS does not allow us to distinguish between the two distinct solid states of the system. We have therefore conducted a series of small-angle light scattering (SALS)

(58) Shalkevich, A.; Crassous, J.; Osman, M.; Schurtenberger, P. Particle sizing in clay suspensions, in preparation.

(59) Kratky, O.; Porod, J. Diffuse small-angle scattering of x-rays in colloid systems. *J. Colloid Sci.* **1949**, *4* (1), 35−70.

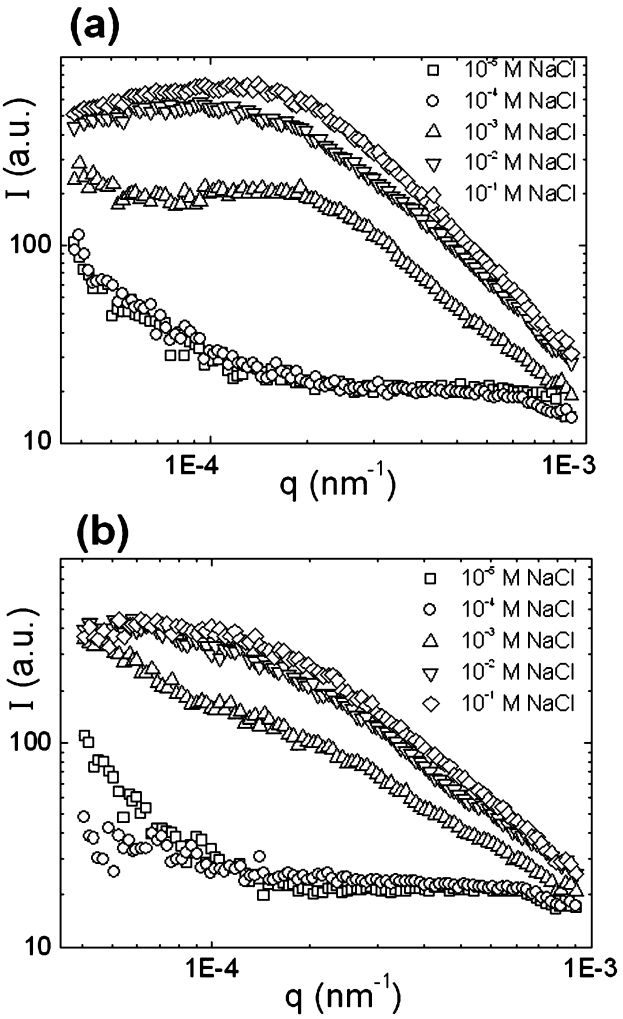


**Figure 5.** Small-angle light scattering data collected for Cloisite CNa suspensions at (a) 1 wt % and (b) 2 wt % and different salt concentrations.

experiments with the same samples at 1 and 2 wt % clay concentrations that have already been investigated with SANS.

**C. Small-Angle Light Scattering.** Small-angle light scattering data from montmorillonite dispersions at 1 and 2 wt % and a salt content varying from $10^{-5}$ to 0.1 M are plotted in Figure 5. Particular care has been taken to measure all samples at the same aging time of 3 months after the preparation of the dispersions. At the very large length scales accessible with SALS, we now observe distinctly different features for the different samples. At the lowest salt concentration of $10^{-5}$ M NaCl and at a Cloisite concentration of 1 wt %, the sample is in a dynamically arrested state. Here, the SALS data exhibit a clear plateau that appears to cross over to the asymptotic power law dependence at higher $q$-values and an upturn at low $q$-values that indicates the existence of large-scale inhomogeneities. A similar behavior can also be seen for the liquidlike samples at $10^{-4}$ and $10^{-3}$ M NaCl. While the characteristic shape and thus the cluster size for $10^{-4}$ M are quite similar to those for the solidlike sample at $10^{-5}$ M, the plateau is, however, shifted to lower values of $q$ for the higher salt concentration, and there is only a weak upturn visible at low $q$-values. The combination of SANS and SALS now allows us to draw some more quantitative conclusions about the structures of the liquid- and solidlike dispersions at low ionic strength. In all these samples, we observe fractal clusters of individual clay platelets, and the cluster size appears to increase with increasing salt concentration. We can try to estimate the average cluster size by applying a form factor for fractal clusters frequently used to analyze data obtained for aggregates that form in reaction- or diffusion-limited cluster growth, the so-called Fisher−Burford equation,

$$I(q) = I(0)\left[1 + \left(\frac{2}{d_F}\right)q^2R_G^2\right]^{-d_F/2} \quad (1)$$

where $R_G$ is the radius of gyration of the scatterer. This equation generalizes the Guinier form to fractal objects and is often used for describing the scattering from fractal gels or clusters.[60−62] In analyzing the data, we fixed the value of $d_F \approx 2.5$, in agreement with the power law regime of the SANS data, while $I(0)$ and $R_G$ were varied in the fitting procedure. This procedure yields a value of $R_G \sim 400-600$ nm for both the dynamically arrested sample at low ionic strength and the liquidlike sample close to the dynamical arrest line at $10^{-4}$ M NaCl. For $10^{-3}$ M NaCl, we find the radius of gyration to dramatically increase to $R_G \sim 3$ $\mu$m. It is clear that this data evaluation is rather qualitative, as we completely neglect possible influences from intercluster interactions, which we know to be present due to the arrest transition that occurs for salt concentrations below $10^{-4}$ M NaCl. Moreover, the data from the liquidlike sample exhibit a possible weak "correlation hole" followed by a weak interaction peak at low $q$-values, once again showing the importance of intercluster interaction effects in any attempt to quantitatively analyze these data. Nevertheless, we believe that, due to the large polydispersity in this system, the crossover to the power-law regime gives at least a semiquantitative estimate of the characteristic length scale of the clusters that form under these conditions. At a high ionic strength, the appearance of the data once again changes. We now observe a well-defined, broad peak at low $q$-values, whose position moves to larger $q$-values with increasing salt concentrations. It is interesting to note that a qualitatively similar behavior can be observed both for the high ionic strength solid and for the phase-separated samples in the initial period of phase separation.

The data obtained with the same ionic strength values but with a higher clay concentration of 2 wt % are reported in Figure 5b. All these samples are now in the solid region of the state diagram. However, both the SANS data reported in Figures 3 and 4 and the SALS data in Figure 5b exhibit small but characteristic differences. The data for the lowest salt concentrations of $10^{-5}$ and $10^{-4}$ M NaCl are consistent with a solid formed by clusters of individual clay particles, where the clusters possess a quite pronounced local order and a rather dense fractal structure. Obviously, these clusters are rather polydisperse, as they do not induce strong positional correlations found in other cluster fluids at low ionic strength,[7] and the resulting cluster solid seems to have large-scale inhomogeneities, as evidenced by the upturn of the intensity at low $q$-values.

At $10^{-3}$ M NaCl, the solid is still made of individual and fully exfoliated clay particles with a weak local order. However, the fractal region now extends far into the SALS regime, and there is only a very faint indication of a Guinier regime of individual clusters, immediately followed by another pronounced upturn at low $q$-values. Finally, for the highest two salt concentrations of $10^{-2}$ and $10^{-1}$ M NaCl, the individual clay particles have lost their local order and are no longer fully exfoliated, but they form a fractal structure based on percolated stacks of clay particles.

(60) Rojas, L. F.; Vavrin, R.; Urban, C.; Kohlbrecher, J.; Stradner, A.; Scheffold, F.; Schurtenberger, P. Particle dynamics in concentrated colloidal suspensions. *Faraday Discuss.* **2003**, *123* (35), 648−687.

(61) Fisher, M. E.; Burford, R. J. Theory of Critical-Point Scattering and Correlations. I. The Ising Model. *Phys. Rev.* **1967**, *156* (2), 583−622.

(62) Sorensen, C. M. Light Scattering by Fractal Aggregates: A Review. *Aerosol Sci. Technol.* **2001**, *35* (2), 648−687.

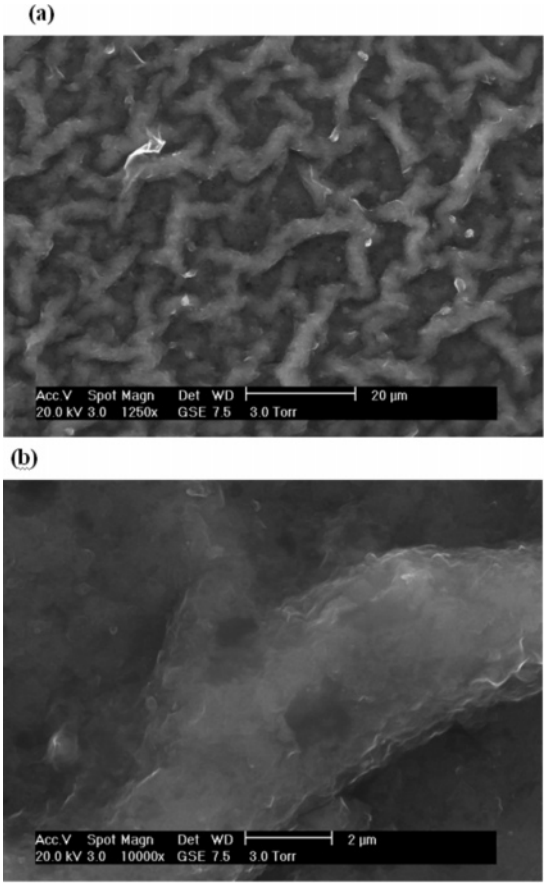


**Figure 6.** Environmental scanning electron microscopy images of a Cloisite CNa suspension at an initial CNa content of 2 wt % (see details in text) and $10^{-3}$ M NaCl, demonstrating the existence of a networklike structure on a micrometer length scale. Scaling bar: (a) 20 $\mu$m and (b) 2 $\mu$m.

The fractal structure also extends far into the SALS regime, and there is an indication of a weak peak at low values of $q$, but the position is at the lower limit of the SALS instrument.

The formation of large concentrated domains at high particle and salt concentrations is also demonstrated in Figure 6, where we show results from environmental scanning electron microscopy (ESEM) of a sample with an initial clay concentration of 2 wt % and a salt concentration of $10^{-3}$ M NaCl. ESEM differs from conventional SEM as the sample is not viewed under high vacuum and, consequently, drastic drying of the sample is avoided. However, some water evaporation of the clay dispersion still occurs, and the sample composition, therefore, is shifted to the upper-right part of the phase diagram. While we can only estimate the final clay concentration to be ~4−5 wt %, this technique nevertheless provides unique direct qualitative information on the undistorted colloidal superstructure. The ESEM images reveal a montmorillonite suspension texture on the micrometer length scale with large clay-poor regions (dark areas), with an average size of ~10 $\mu$m, and a network of ~3 $\mu$m diameter clay-rich areas (bright network structures). The existence of similar microdomains in laponite suspensions was already hypothesized by Levitz et al. based on USAXS measurements.[25]

## Discussion

Our investigation has provided us with detailed information on the structures of solid- and liquidlike clay dispersions as a function of ionic strength over an extended range of length scales from a fraction of a nanometer up to many micrometers using a combination of SANS and SALS. While these experiments are not able to distinguish between solid- or liquidlike behavior, they provide us with information that now allows us to propose a rather detailed model for the structures underlying the different regimes of the state diagram in Figure 1. This model is schematically illustrated in Figure 7.

At the lowest Cloisite concentrations and at low ionic strength, the SANS data clearly demonstrate that the individual clay particles are fully exfoliated. However, the comparison with the calculated form factor for polydisperse discs also reveals that the Cloisite particles are not individually dispersed but that they form quite extended clusters with a radius of ~400−600 nm as seen from the combination of SANS and SALS (Figure 7a and c). It is obvious that the possible existence of clusters that reappear directly after sonication is not only of considerable importance in fundamental colloid physics but also of utmost importance for the use of these colloidal particles in applications such as nanocomposites.

The formation of equilibrium clusters as a result of a balance between short-range attraction and long-range repulsion has recently been described for a number of colloidal suspensions and protein solutions, and their existence has also been demonstrated by computer simulation.[7,63−69] The interplay of opposing forces, that is, the coexistence of a short-range attraction and a weakly screened and thus long-range electrostatic repulsion, provides the stabilizing mechanism for these equilibrium structures. The attractions can be seen as an effective surface tension that leads to a decrease in surface energy upon clustering and thus represents the driving force for the controlled self-assembly. At a certain cluster size, the increased Coulomb energy of the cluster compensates the gain in surface energy and hence prevents the cluster from further, unlimited growth. We can imagine that a similar mechanism is also responsible for the cluster formation observed with Cloisite at low ionic strength. At the conditions chosen, the platelet faces carry a significant number of charges. Cluster formation is therefore caused by the combination of a weakly screened Coulomb repulsion between the platelet faces that stabilizes the cluster and an attractive interaction that acts as the driving force for clustering. This attraction arises from the combined effect of an electrostatic contribution due to the oppositely charged platelet faces and edges and a strong van der Waals attraction. However, it is clear that we currently do not have a good quantitative understanding of the complex interaction potential between the clay particles and that additional investigations are required.

The pronounced correlations between the particles seen by SANS at low ionic strength and the intermediate $q$-values indicate ordering of the clay particles on characteristic distances of ~70−100 nm, where the typical distance between the particles increases with decreasing Cloisite concentration. While the SANS patterns

(63) Campbell, A. I.; Anderson, V. J.; van Duijneveldt, J. S.; Bartlett, P. Dynamical Arrest in Attractive Colloids: The Effect of Long-Range Repulsion. *Phys. Rev. Lett.* **2005**, *94* (20), 208301.
(64) Sedgwick, H.; Egelhaaf, S. U.; Poon, W. C. K. Clusters and gels in systems of sticky particles. *J. Phys.: Condens. Matter* **2004**, *16* (42), S4913.
(65) Mladenovic, I. L.; Kegel, W. K.; Bomans, P.; Frederik, P. M. Observation of Equilibrium, Nanometer-Sized Clusters of Silver Iodide in Aqueous Solutions. *J. Phys. Chem. B* **2003**, *107* (24), 5717−5722.
(66) Groenewold, J.; Kegel, W. K. Anomalously Large Equilibrium Clusters of Colloids. *J. Phys. Chem. B* **2001**, *105* (47), 11702−11709.
(67) Groenewold, J.; Kegel, W. K. Colloidal cluster phases, gelation and nuclear matter. *J. Phys.: Condens. Matter* **2004**, *16* (42), S4877.
(68) Sciortino, F.; Mossa, S.; Zaccarelli, E.; Tartaglia, P. Equilibrium Cluster Phases and Low-Density Arrested Disordered States: The Role of Short-Range Attraction and Long-Range Repulsion. *Phys. Rev. Lett.* **2004**, *93* (5), 055701.
(69) Mossa, S.; Sciortino, F.; Tartaglia, P.; Zaccarelli, E. Ground-State Clusters for Short-Range Attractive and Long-Range Repulsive Potentials. *Langmuir* **2004**, *20* (24), 10756−10763.

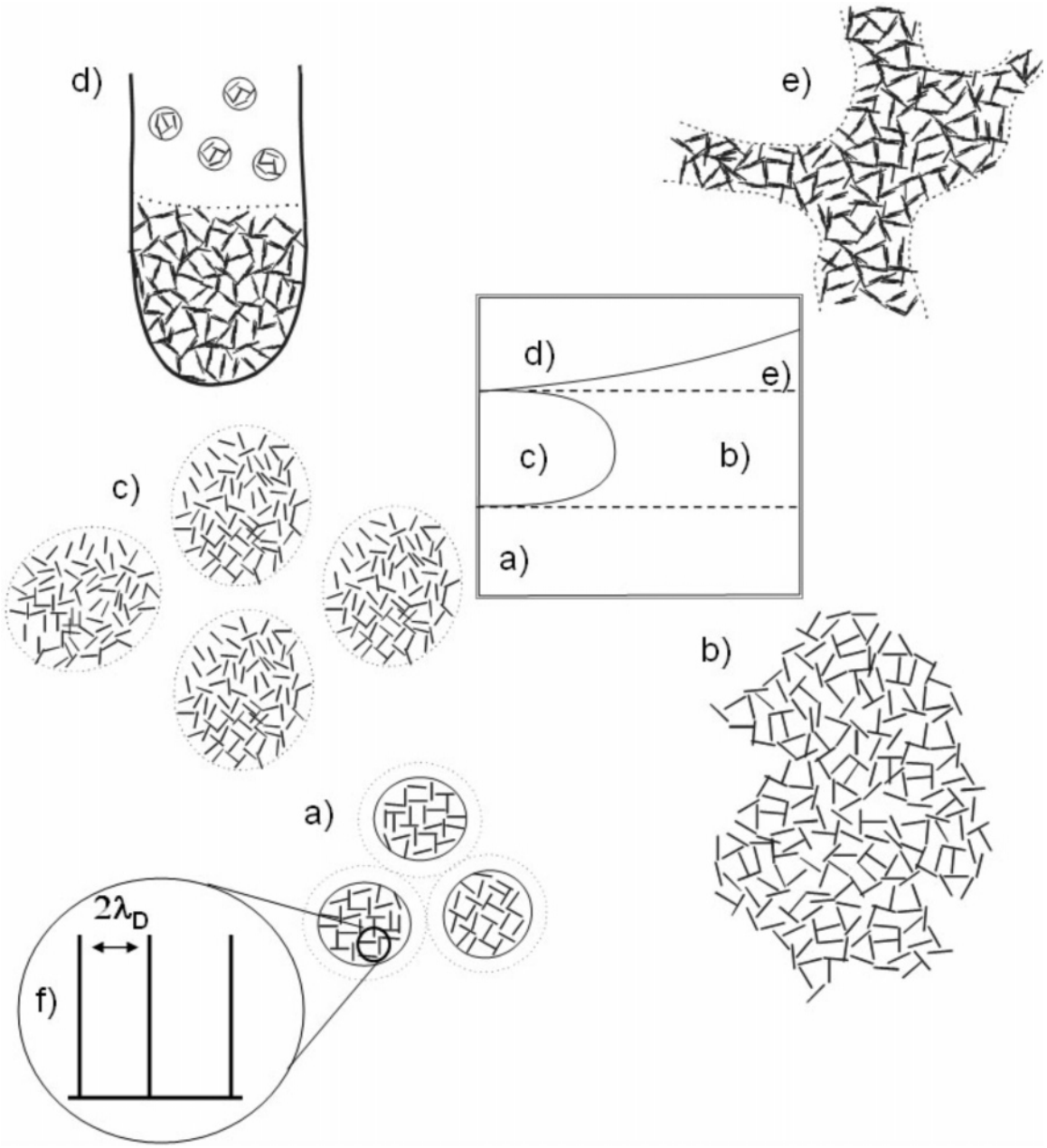


**Figure 7.** Schematic representation of the different states of the aqueous clay suspensions: (a) Wigner glass containing clusters with a size of 400−600 nm and a high degree of internal ordering. (b) Continuous percolation gel with a random orientation of the individual discs. (c) Cluster fluid formed by percolation clusters with a size of 3−5 $\mu$m and a random orientation of the individual discs. (d) Phase-separated sample with a weak percolation gel formed by small stacks of clay particles on the bottom and a few smaller clusters on the top. (e) Transient gel formed by concentrated domains of a percolation gel of small stacks of platelets. (f) Structure of the unit cell inside a cluster in the Wigner glass.

are distinctly different from the typical nematic pattern previously seen at higher particle concentrations for other clays,[70] they still indicate that the individual platelet faces are at least partially ordered in some sort of a house-of-cards structure that would allow minimization of the repulsive Coulomb energy. The proposed "unit cell" of such an ordered domain inside the clusters is shown in Figure 7f. The overall structure of the clusters appears to be characterized by a power law behavior of the scattered intensity over at least 2 orders of magnitude in $q$, indicating a rather dense but fractal-like interior structure of the clusters. A fractal exponent of 2.5 is, in fact, in agreement with random percolation, which provides a likely basis for the description of the clusters as the result of a percolated structure of partially ordered house-of-cards-type domains.

Based on the characteristic distance derived from the weak structure factor peak and using a simple house-of-cards structure for the "unit cell" inside the clusters and the average cluster radius obtained from SALS, we can try to estimate the number of particles per cluster and subsequently the effective cluster volume fraction. These numbers depend on the Cloisite concentration and on the Debye length $\lambda_D$, as $\lambda_D$ will act as an interaction distance that will effectively increase the volume fraction of the particles and thus determine the onset of dynamical arrest. The effective volume fraction of the clusters is

$$\varphi_{cl} = \frac{V_{cl}}{V} \qquad (2)$$

(70) Martin, C.; Pignon, F.; Magnin, A.; Meireles, M.; Lelievre, V.; Lindner, P.; Cabane, B. Osmotic Compression and Expansion of Highly Ordered Clay Dispersions. *Langmuir* **2006**, *22* (9), 4065−4075.

where $V_{cl}$ is the effective volume occupied by the clusters and $V$ is the overall volume of the system. The effective total volume occupied by the clusters is

$$V_{cl} = v_{cl}N_{cl} \quad (3)$$

where $v_{cl}$ is the effective volume of an individual cluster and $N_{cl}$ is the number of clusters in the system. The number of clusters is

$$N_{cl} = \frac{N_{pl}}{N_{pl/cl}} \quad (4)$$

where $N_{pl}$ is the total number of platelets in the dispersion and $N_{pl/cl}$ is the number of platelets in an individual cluster. The number of platelets in the dispersion is given by

$$N_{pl} = \frac{V_{pl}}{v_{pl}} = \frac{V\varphi_{pl}}{v_{pl}} \quad (5)$$

where $\varphi_{pl}$ is the geometrical volume fraction of the platelets, $V_{pl}$ is the total volume of the platelets, and $v_{pl}$ is the volume of an individual platelet. With this, eq 2 then becomes

$$\varphi_{cl} = \frac{v_{cl}\varphi_{pl}}{v_{pl}N_{pl/cl}} \quad (6)$$

If we assume a cluster to be a cube of 600 nm length and at a characteristic distance of 100 nm between two platelet faces, this leads to a total number of $3^3 = 27$ unit cells with 4 platelets per cell. If we take into account that some of the platelets are shared by a second unit cell inside the cube, which leads to a correction factor of $^3/_4$, we then obtain a total number $N_{pl/cl}$ of 80 particles per cluster ($^3/_4 \times 4 \times 27$). The volume of an individual platelet with a radius of 100 nm and a thickness of 1 nm is $v_{pl} = \pi R^2 h = 3.14 \times 10^4$ nm$^3$. Taking into account the effective size of the clusters $l_{cl,eff}$ as $l_{cl,eff} = l_{cl} + 2\lambda_D = 600 + 100 = 700$ nm, the effective volume of the individual cluster is $v_{cl} = {}^4/_3\pi(l/2)^3 = 1.8 \times 10^8$ nm$^3$. Finally, the platelet volume fraction can be obtained for the weight concentration (2 wt %) and the known density (2.66 g/mL), which leads to $\varphi_{pl} = 7.7 \times 10^{-2}$. Using the proposed structure model and the estimated cluster size, eq 6 then yields an effective cluster volume fraction of ~0.55. This is quite close to the value of the glass transition published for hard spheres and indicates that the arrested systems at low ionic strength correspond to a repulsive "Wigner glass", where the clusters act as effective hard spheres with a hard sphere radius given by the sum of the cluster radius and the Debye length.

With increasing salt concentration, the Debye length decreases, and subsequently both the packing density as well as the cluster radius and mass increase as a consequence of the reduced repulsive Coulomb energy of the clusters. This is consistent with the higher absolute neutron scattering intensity (Figure 3a−c) and the SALS data (Figure 5a), where the Guinier regime has shifted to lower $q$-values. However, the decrease of $\lambda_D$ and the subsequent decrease in the effective cluster volume fraction still dominates, which leads to the melting of the cluster glass and the formation of a cluster fluid. At the same time, the structural correlation inside the clusters disappears, and the local structure becomes disordered (Figure 7c). For the 1 wt % clay suspension, the transition point is very close to $10^{-4}$ M NaCl, where we observe only minor variations in cluster size and density but dramatic changes in the rheological behavior. The liquidlike behavior does, in fact, persist up to an ionic strength close to $10^{-2}$ M NaCl, despite the fact that the average cluster size considerably increases as a result of the modified balance between attraction and screened Coulomb repulsion. A similar behavior has, in fact, also been observed for cluster-forming protein solutions.[7] However, if, at a constant ionic strength of $10^{-3}$ M NaCl, the Cloisite concentration now increases, the subsequent growth of the clusters becomes dominant and results once again in a liquid−solid transition. The underlying structure now corresponds to the formation of a homogeneous percolation gel (or attractive particle glass) rather than a Wigner cluster glass, as can be seen from the combination of SANS (Figure 3a) and SALS (Figure 5b).

The situation once again changes completely if we go to even higher salt concentrations. At the lowest Cloisite concentration of 1 wt %, this then first leads to a solid formation at $10^{-2}$ M NaCl, where the structure now corresponds to a percolation gel formed by small stacks of individual discs. This transition from a Wigner glass at $10^{-5}$ M NaCl to a percolation gel at $10^{-2}$ M NaCl is also supported by the dramatic change in the elastic modulus observed in Figure 2b. At a salt concentration of 0.1 M NaCl, the sample then becomes completely destabilized and we find phase separation with a flocculated, solidlike phase in the bottom phase and a dilute, liquidlike suspension in the top phase.

The scattering experiments allow us to further elucidate the underlying mechanisms and resulting structures. They were done in the initial stage of the phase separation, where the samples still look perfectly homogeneous on macroscopic length scales as monitored by visual inspection. The first obvious observation made from the SANS experiments (shown in Figure 3c and d) is the fact that the individual clay particles are no longer completely exfoliated but that they rather form small stacks of particles. On larger length scales, the overall structure still shows the signs of a dense percolated network of these stacks. However, the SALS data shown in Figure 5a reveal a distinctly different low-$q$-value behavior with the formation of a peak that resembles spinodal decomposition for both the solidlike and the phase separating sample. Obviously, the Coulomb repulsion is now so strongly screened that the samples become unstable and tend to aggregate and phase separate. The concentrated phase then forms a percolated network with stacks of individual Cloisite discs as the building blocks, and the top phase corresponds to a dilute cluster suspension. However, at the lower end of this aggregation−phase separation regime, the larger spinodal-like structures apparently arrest, and the system forms a (transient) gel where a solidlike bicontinuous network composed of a dilute cluster phase and an arrested percolated phase exists. The extension of the transient gel increases with increasing Cloisite concentration (Figure 7), and at the same time, the resulting domain size is much larger (Figure 5b) as dynamical arrest appears to occur earlier in the phase separation process. The existence of a connected backbone of concentrated domains is also in agreement with our ESEM observations (Figure 6). Such a scenario is indeed comparable to the description of viscoelastic phase separation and its competition with transient gel formation discussed in detail by Tanaka and collaborators.[71,72] The fact that we find the coexistence of a self-similar relationship at intermediate $q$-values with a correlation peak at low and high $q$-values may, at first, look surprising. However, a situation where self-similarity and correlation effects coexist at different length scales is, in fact, very often encountered in colloidal systems and also is already very well-documented. Good examples are dilute colloidal gels formed via diffusion-limited aggregation that exhibit a correlation peak at low $q$-values, reflecting the cluster size that represents

(71) Tanaka, H.; Nishikawa, Y.; Koyama, T. Network-forming phase separation of colloidal suspensions. *J. Phys.: Condens. Matter* **2005**, *17* (15), L143.

(72) Tanaka, H.; Koyama, T.; Araki, T. Network formation in viscoelastic phase separation. *J. Phys.: Condens. Matter* **2003**, *15* (1), S263.

the building blocks of the gel, a self-similar cluster structure at intermediate distances, and again a monomer−monomer correlation peak at short distances.[73]

A comparison between our postulated state diagram in Figure 7 and the phase diagram for Laponite previously proposed by Tanaka and collaborators indeed reveals at least a qualitative agreement.[17] While the phase diagram of Tanaka et al. was largely based on indirect evidence from a number of different sets of experimental data from the literature, we have now been able to come up with a rather detailed description of the underlying suspension structure over a very large range of length scales and for a systematic variation of clay and salt concentrations. This has also led to a modified picture for the Wigner glass and the fluid phase observed at low volume fractions and ionic strength, where the building blocks are particle clusters and not individual clay platelets. Moreover, we have also been able to demonstrate the impact of ionic strength on the local structure, where we observed a transition from ordered to randomly oriented individual platelets and finally to the formation of small stacks of discs with increasing ionic strength.

## Conclusion

The question of cluster formation and dynamical arrest in clay particle suspensions is of considerable importance in fundamental colloid physics. Aqueous clay suspensions are fascinating model systems to study fundamental problems in colloid science, and they have recently attracted particular attention in the colloid community. An interesting feature of clay suspensions is the existence of interactions at different length scales combined with the anisotropic structure of the particles, which lead to a variety of structural and dynamic phenomena such as orientation, ordering, and clustering (house-of-cards-like) as a function of the particle concentration ($c$) and of the ionic strength ($I_0$). To understand the relationship between the local and macroscopic properties and the structures of clay suspensions, we have thus systematically investigated the phase and state diagrams of clay particles in water. We, in particular, focused on sodium Cloisite (CNa) particles at concentrations typically used in nanocomposites (concentrations from 1 to 4 wt %) and at an extended range of ionic strengths ($10^{-5}$−$10^{-1}$ M NaCl). The suspensions have been characterized using rheology and a combination of scattering techniques (neutrons, light) that allowed us to cover an enormous range of length scales from local structural details at almost atomistic resolution to superstructures that are many micrometers in size.

The resulting state diagram has shown a close resemblance to the theoretical diagram previously postulated for Laponite suspensions. We have, in particular, been able to confirm the existence of a repulsive (Wigner) cluster glass that melts with increasing salt concentration and is finally transformed into an arrested percolated network of concentrated clay domains or a phase-separated flocculated phase at high ionic strength. At higher clay concentrations, we have been able to directly demonstrate the subtle structural changes that accompany the transition from a repulsive cluster glass at low ionic strength to an attractive glass of percolated individual clay platelets at intermediate ionic strength to a gel formed by an arrested network of percolated small stacks of clay platelets at high ionic strength. This investigation once again demonstrates the quite universal nature of the sequence of arrested states already investigated for spherical colloids.[74−76] It is clear that we still lack additional data on the evolution of the dynamic properties as a function of concentration, ionic strength, and aging time for the same system. Moreover, a comparison with detailed computer simulations would also be extremely interesting. Nevertheless, we believe that we have been able to provide further insight into the phenomenon of dynamical arrest in platelet suspensions that is both of considerable interest for the colloid community and of enormous technological importance for a wide variety of applications.

**Acknowledgment.** We thank Massud Dadras for his help with the ESEM experiment. This work is based, in part, on experiments performed at the Swiss spallation neutron source SINQ, Paul Scherrer Institute (PSI), Villigen, Switzerland. We gratefully acknowledge the expert help of our local contacts at PSI, Joachim Kohlbrecher and Ronny Vavrin. We are deeply grateful for precious and fruitful discussions with Veronique Trappe, Brian Vincent, and Jeroen van Duijneveldt. This work was supported by the Swiss National Science Foundation, the State Secretariat for Education and Research (SER) of Switzerland, and the Marie Curie Network on Dynamical Arrest of Soft Matter and Colloids (MRTN-CT-2003-504712).

(73) Rottereau, M.; Gimel, J. C.; Nicolai, T.; Durand, D. Monte Carlo simulation of particle aggregation and gelation II. Pair correlation function and structure factor. *Eur. Phys. J. E* **2004**, *15*, 141−148.

(74) Sciortino, F. Disordered materials: One liquid, two glasses. *Nat. Mater.* **2002**, *1*, 145.

(75) Dawson, K. A. The glass paradigm for colloidal glasses, gels, and other arrested states driven by attractive interactions. *Curr. Opin. Colloid Interface Sci.* **2002**, *7* (3−4), 218−227.

(76) Mezzenga, R.; Schurtenberger, P.; Burbidge, A.; Michel, M. Understanding foods as soft materials. *Nat. Mater.* **2005**, *4* (10), 729−740.